

Measurement methods of interparticle interactions via optical laser tweezers and quantification of their effects on oil-water interface morphologies

Lee, Ha eun¹; Hong, In Ki^{*};

¹Skin Care R&D Lab. Kolmar Korea, 61, Heolleung-ro 8-gil, Seocho-gu, Seoul, Republic of Korea

*Skin Care R&D Lab. Kolmar Korea, 61, Heolleung-ro 8-gil, Seocho-gu, Seoul, Republic of Korea, +82 010-5018-9789, inkiaaa@kolmar.co.kr

Abstract

Colloidal particles are irreversibly attached to fluid-fluid interfaces. Such adsorption is depends on the surface charges, wettability, and characteristic of trapped particles. Adsorption of solid particles decreases the interfacial tension and consequently stabilizes the interface. Accordingly, solid particles can be good alternatives to replace molecular surfactants. The behaviors of interface-trapped particles and their assembled structures at the interfaces are affected by two competing interactions: electrostatics and capillarities. Typically, the electrostatics interactions effectuate repulsions of the particles due to asymmetric charge distribution across the interface, whereas the capillary interactions lead to attractions to stabilized the system by minimizing the surface free energy. Since the relative strength between these interparticle interactions determines the assembled colloidal microstructures and their rheological properties, it is significant to quantitatively investigate the electrostatic and capillary interactions. In the context of fundamentally understanding the effect of particle size on the interparticle interactions, we fabricate polystyrene particles with controlled size distributions via the microfluidic method, and measure the interactions of between the particles with different dimensions using optical laser tweezers.

Keywords: Oil-Water interface, Electrostatic interaction, Capillary interaction, Optical laser tweezers

Introduction.

Charged particles trapped at a fluid-fluid interface typically experience two competing interactions: electrostatic and capillary [1-6]. For instance, when colloidal particles of micrometer dimensions are adsorbed to an interface [7, 8], electrostatic repulsion occurs due to asymmetric distribution of dissociated surface charges and counterions across the interface [9-11]. Capillary interactions are caused by excess interface surface area, which is caused in turn by interface deformation around individual particles [12-18]. When two interface-trapped particles are within a sufficiently small neighborhood, they spontaneously migrate toward one another to decrease the excess area. Accordingly, equilibrium microstructures and corresponding rheological properties of such particle-laden interfaces inevitably depend on the relative strengths of the two interactions. When electrostatic repulsion is stronger than capillary attraction, the particles tend to form triangular lattice structures with finite interparticle separations [19-23]. In the alternative case, the strong capillary attraction induces aggregation of the particles, resulting in percolated microstructures [24-33]. Such particle-interface systems have been intensively investigated and exploited over a broad range of applications [1, 34-40], such as food, cosmetics, drug delivery, oil/water recovery processes, phase transfer catalysts, and stabilization enhancement of complex fluid systems.

Capillary interactions between particles floating at a fluid-fluid interface can be either repulsive or attractive depending on the local shape of the interface deformation around each particle and the relative orientations between the particles [14, 41-45]. For two particles that can freely rotate horizontally at the interface, the surface free energy is always minimized by an attractive capillary interaction. In general, typical spherical microbeads with surface charges dominantly exhibit electrostatic repulsion, while the magnitude of capillary attraction is relatively small. Electrostatics can be suppressed by adding a significant quantity of electrolytes and/or surfactants; electrolytes screen the surface charge effects in the aqueous phase, and molecular surfactants alter the wettability of the particles at the interface [17, 21, 30]. In such conditions, in which electrostatics are suppressed, capillary interaction of the micrometer-sized particles is mainly induced by the undulated interface meniscus around individual particles [12, 14]. The interface undulation is attributed to non-homogeneous surface properties of the particles [46, 47]. After fitting the undulated interface using a multipole expansion, the lowest stable pole is found to be the quadrupole, while the effects

of other higher poles (e.g., hexapole, octapole, etc.) on capillary interaction are negligible [12, 14]. The capillary attraction force between two particles with quadrupolar interface deformation decays as $F_{quad} \sim r^{-5}$, where r is the center-to-center separation. This scaling exponent has been also experimentally demonstrated for quadrupolar capillary force for particles with diameters of a few micrometers over long-range separations [13, 26, 41, 42, 48].

Note that the effect of gravity on interface deformation likely becomes significant as particle size increases [16, 49-52]. Gravity pulls the particle downward against the interfacial tension force that tends to flatten the interface. The ratio of the two forces corresponds to the Bond number, expressed as $Bo = \frac{R^2 g(\rho_B - \rho_A)}{\gamma_{AB}}$, where g is gravitational acceleration, R is particle radius, γ_{AB} is the interfacial tension between A and B fluids, and ρ_A and ρ_B are the respective densities of superphase A (e.g., oil) and subphase B (e.g., water) [1]. Therefore, when the Bond number is sufficiently small ($Bo \ll 1$), the gravity-induced capillary force can be considered negligible. A simple calculation for a particle with $2R = 1$ mm at an oil–water interface with $\gamma_{ow} = 50$ mN/m results in the Bond number of O(-3). Technically, this result suggests that particles can remain as singlets without forming aggregates when they experience sufficiently strong electrostatic repulsion. However, the Bond number argument is apparently inconsistent with experimental observations by Monteux et al., in which polystyrene (PS) particles with $2R \approx 8.7$ μm formed an aggregated network [53]. It was suggested that the attractions could be attributed to gravity-induced capillary force. Alternatively, it was reported that PS particles with $2R \approx 200$ μm , surface-stabilized by polyvinyl alcohol, organized into unique patterns at a curved oil–water interface due to strong electrostatic repulsion [54-56].

Materials and Methods.

Optical laser tweezers

The optical laser apparatus was built with an inverted microscope (Nikon Ti-U, Japan). To optically trap individual PS particles of diameter $2R \approx 3 \mu\text{m}$, the time-sharing optical trapping method was used, in which a single laser beam generated multiple traps [41, 42, 57, 58]. A 10 W CW Nd:YAG laser beam (Coherent Matrix, USA) with wavelength 1064 nm passed through an acousto-optic deflector (AOD, Opto-electronic DTSXY-400-1064 2D, USA) and reached a $60\times$ water immersion objective with a numerical aperture (NA) 1.2 (CFI Plan Apo VC 60XC WI, Nikon, Japan) of the microscope. The objective lens converged the laser beam to the focal plane at a large convergent angle, leading to the formation of optical traps at designated positions. The positions of the optical traps could be controlled with the AOD operated by LabVIEW software. To measure the force between PS particles of diameter $2R > 80 \mu\text{m}$ that were fabricated via the microfluidic method, a low NA objective ($4\times$) with NA 0.13 (CFI Plan Fluor, Nikon, Japan) was used to bring two large particles together. In this case, the Gaussian laser beam was widely focused on the focal plane. The laser power was measured in front of the objective lens with an optical power meter (PM100D, Thorlabs, USA).

Force measurement between PS particles at an oil–water interface

Preparation of flow cell

The oil–water interface was formed in a flow cell made of inner and outer cylinders, as used in previous work [42]. The inner cylinder was composed of aluminum and Teflon rings, and the interface was pinned at the junction of the two rings (Figure 1). A circular coverslip (Marienfeld, no.1.5H) was attached to one side of the outer glass cylinder. The small coverslip pieces present between the inner and outer cylinders, acting as glass spacers, provided space for water to pass. The flow cell was placed on the mechanical stage of an inverted microscope (Nikon, Ti-U) with an optical laser apparatus installed. After adding ultrapure water and *n*-decane (Acros Organics) into the flow cell, a diluted particle solution of 30 vol% isopropanol (Sigma-Aldrich) was added to the oil–water interface. Note that, prior to use, *n*-decane was filtered with aluminum oxide particles (Acros Organics, acidic activated, particle size 100–500 μm) to remove any polar impurities. After 30min, the flow cell was sealed with another coverslip using vacuum grease (Dow Corning, USA) to minimize convective

flows. This flow cell was used for directly measuring the interaction force of pairs of particles of diameter $\sim 3 \mu\text{m}$

Direct force measurement

The time-sharing optical laser tweezers were used to individually trap the particles at the oil–water interface formed in the flow cell (Figure 1 and Figure 4) [21]. PS particles with two different functional groups on the surface were used; PS with sulfonate groups (SPS, Invitrogen, USA) and PS with carboxyl groups (CPS, Invitrogen, USA). Particle size was analyzed with a scanning electron microscope (SEM, AIS2000C, Seron Technologies Inc.): 2.96 ± 0.05 for SPS and 3.16 ± 0.07 for CPS. The ζ -potential was measured with a Zetasizer (ZEN3600, Malvern Instruments): -57.5 ± 2.2 for SPS and $-65.6 \pm 3.2\text{mV}$ for CPS. $2 \mu\text{L}$ of a dilute suspension of PS particles in a mixture of water and isopropyl alcohol was dropped on the surface of oil. The particles attached irreversibly to the oil–water interface due to the strong attachment energy [59, 60]. To directly measure the pair interaction force, two particles at the oil–water interface were trapped initially at a far distance (SPS: $r \approx 33 \mu\text{m}$, CPS: $r \approx 40 \mu\text{m}$), at which interactions between them were assumed to be negligible. As one particle was translated stepwise to the other stationary particle, the particles were displaced from their equilibrium positions ($\Delta x = 0$). A microscope image sequence was captured at a rate of 30 frames per second (fps) using a charge-coupled device (CCD) camera (Hitachi, KP-M1AN), and the recorded images were analyzed via ImageJ software [61]. The displacement of the stationary particle Δx determined by image analysis was converted to interaction force as a function of r using $F_{rep}(r) = \kappa_t \Delta x$, in which κ_t represents trap stiffness. Prior to the measurement of pair interaction force, a drag calibration was carried out to obtain the value of κ_t . We refer the reader to the detailed method of drag calibration in previous work.

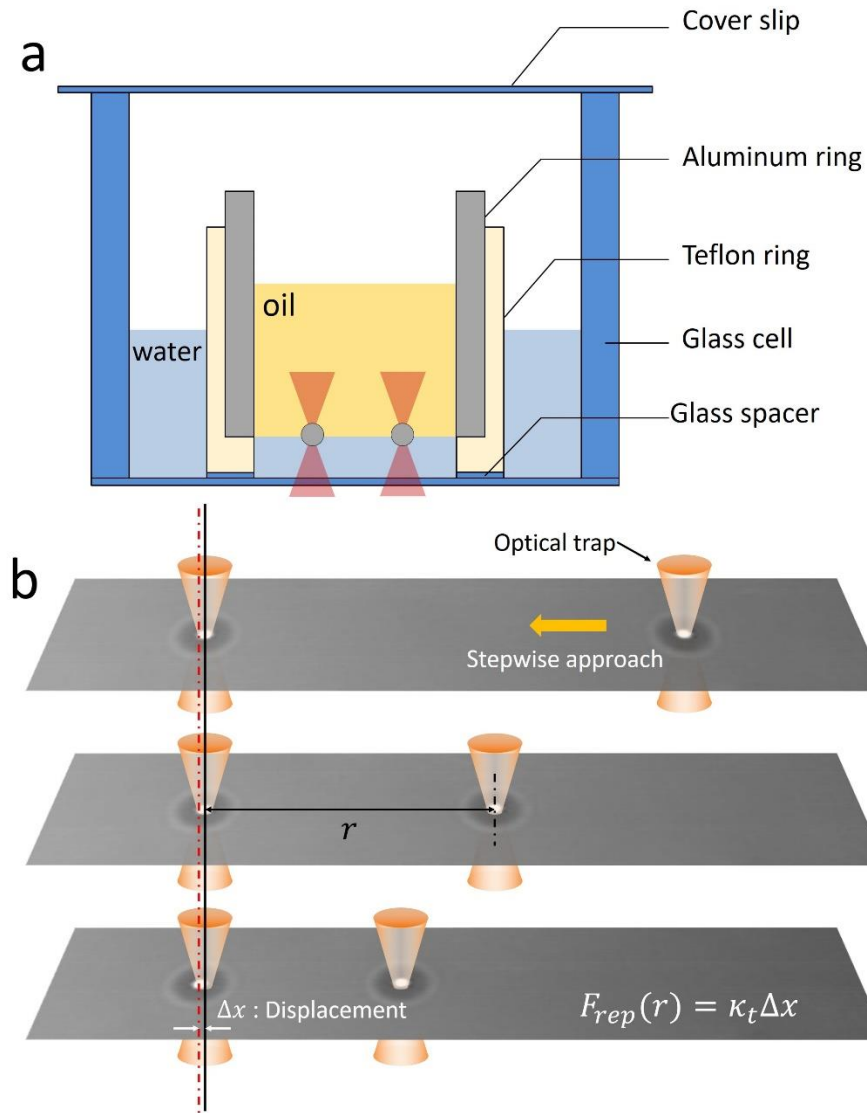


Figure 1. Direct measurements of the interaction force using optical laser tweezers. (a) Schematic of sample flow cell. (b) Optical microscope images for measuring the pair interaction force of PS particles with $2R \approx 3 \mu\text{m}$ at the oil-water interface.

Indirect force measurement

For large PS particles of diameter $2R > 80 \mu\text{m}$, the interparticle force was indirectly measured by applying a widely focused laser beam to the particles [54]. As shown in Figure 2 and Figure 4, the PS particles in water-IPA (1:1 volume ratio) were spread at the surface of water in a petri dish (Falcon, $35 \times 10 \text{ mm}$). After 30 min, the particles at the air-water interface were individually, manually transferred to the surface of another water-filled petri dish using a micropipette. After adding two PS particles at the pristine air-water interface, 1.5 mL of *n*-decane was carefully added to cover the water surface completely. When the widely focused laser beam issued from the $4\times$ objective, the two particles at the oil–water interface began to approach to each other due to the optical gradient force. At a certain separation r , the laser traps were removed by blocking the laser with an infrared (IR) detector card (VRC2, Thorlabs). The particles repelled each other with an initial velocity v_0 due to electrostatic repulsion. The same procedure was repeated multiple times, varying the release separation sequence. All runs were captured at a rate of 30 frames per second (fps) using a CCD camera (Hitachi, KP-M1AN). ImageJ software was used to obtain the distance between the two particles as a function of time t .

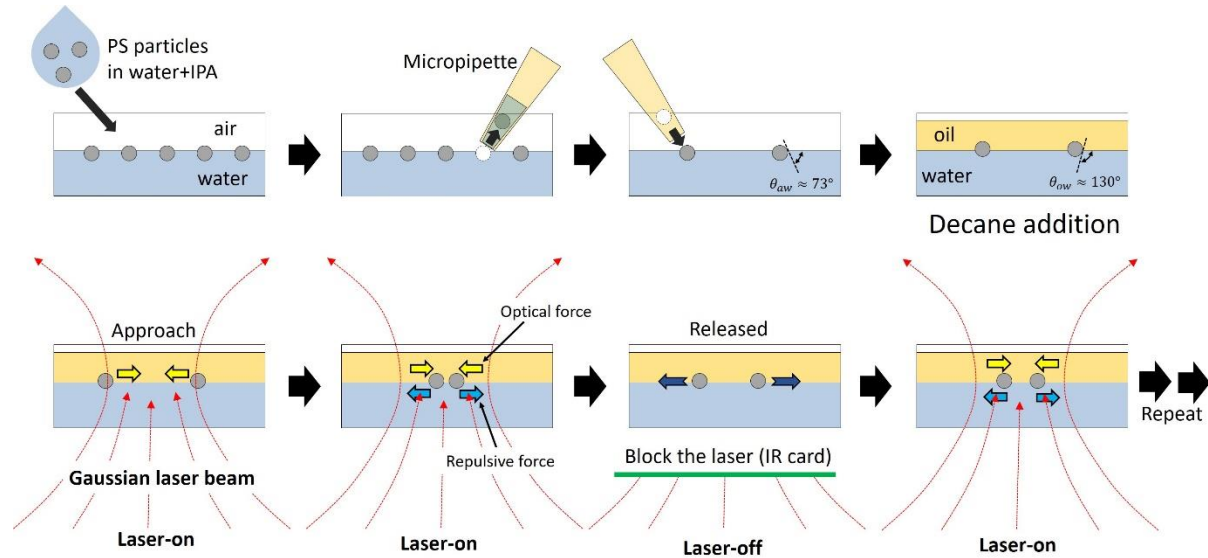


Figure 2. Schematic illustration of indirect force measurement between two large PS particles at the oil–water interface.

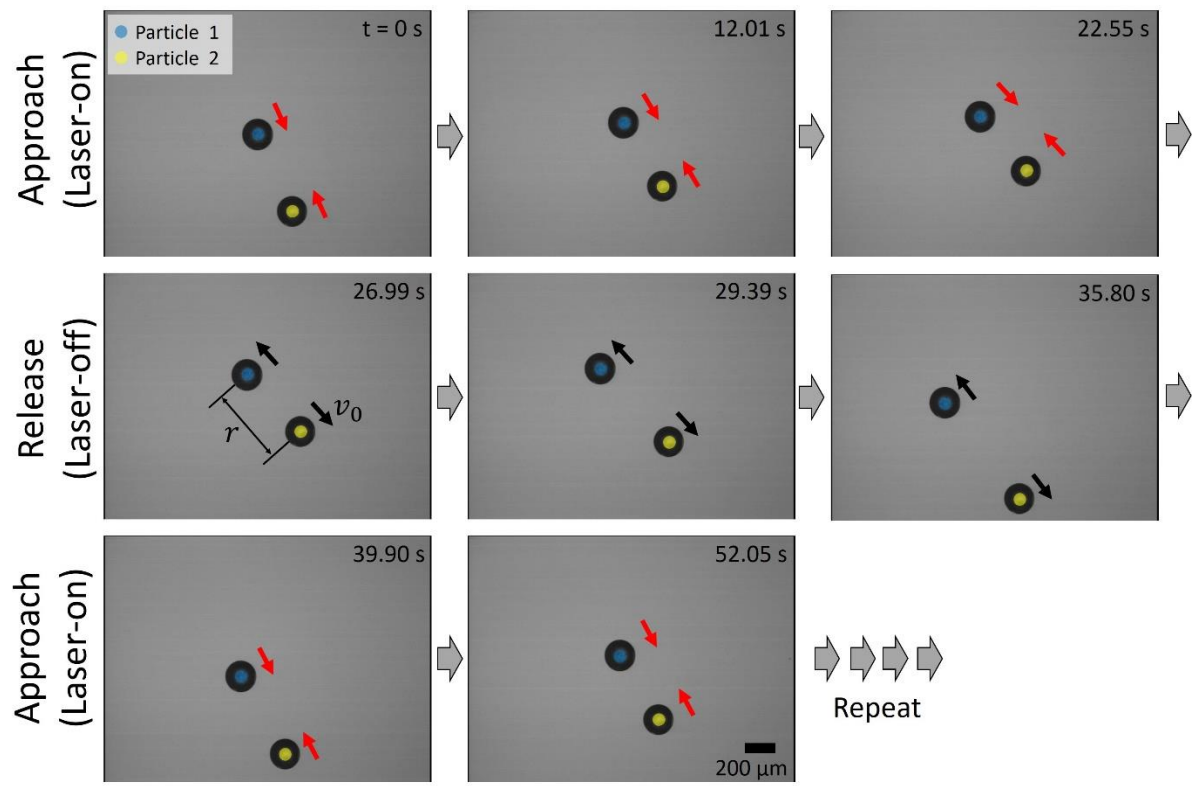


Figure 3. Optical microscope images showing indirect force measurements between two PS particles of diameter $2R \approx 213 \mu\text{m}$. As the laser was repeatedly switched on and then off, the particles approached and then repelled one another. The laser power was $P_{20x} = 11.21 \text{ mV}$.

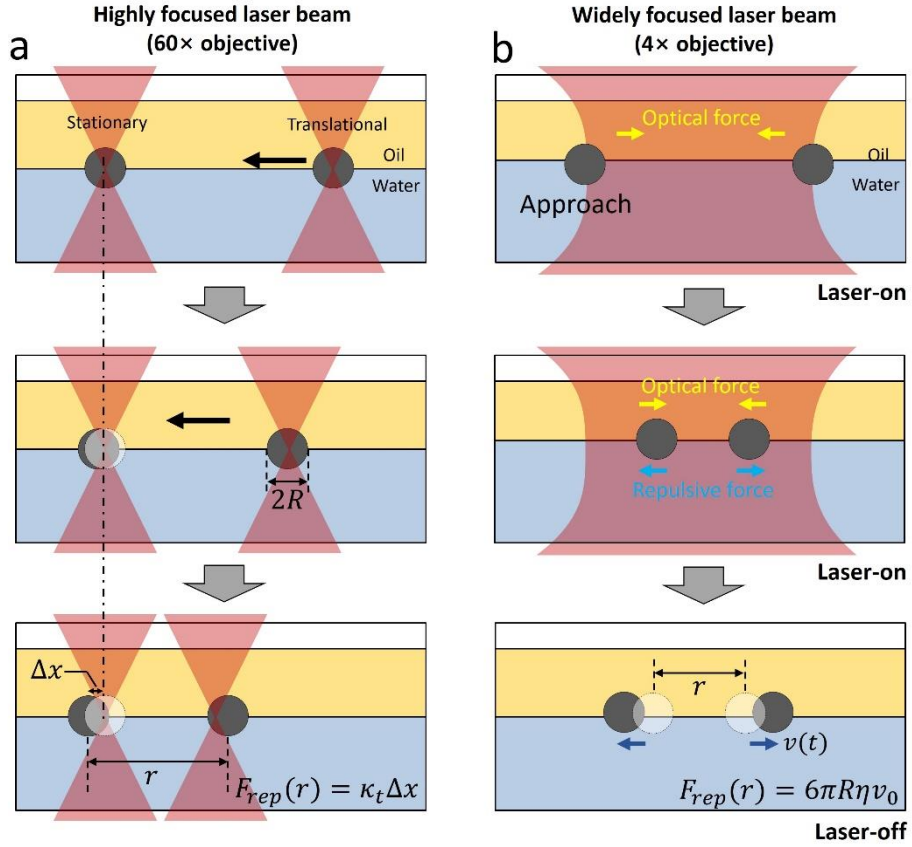


Figure 4. Schematics illustrating measurements of pair interaction forces between two particles at the oil–water interface using an optical laser apparatus. (a) Direct force measurements using time-sharing optical traps, in which the two particles were individually trapped at the interface. The $60\times$ water immersion objective with $NA = 1.3$ generated a highly focused laser beam, leading to the formation of optical traps at the focal plane. One particle was translated toward the other particle held stationary by a trap. The displacement Δx of the stationary particle was converted to pair interaction force (F_{rep}) as a function of the separation r , $F_{rep} = \kappa_t \Delta x$. (b) Indirect force measurements using a widely focused laser beam generated from the $4\times$ objective. Two larger particles at the oil–water interface came closer due to the optical force. At a certain distance, the laser was removed to release the particles. The release velocity $v(t) = v_0$ at the moment of laser-off was determined via image analysis, and the corresponding force was calculated as a function of r using the Stokes drag force equation.

Results and Discussion

Indirect force measurement result

To determine the force between two large PS particles at the oil–water interface, the release velocity was measured immediately after the screening of the laser. As shown in Figure 3, two particles began approaching at the time of laser-on, and began repelling at the time of laser-off. For instance, Figure 5a shows the separation profile as a function of time for a scenario in which the laser was turned on and off three times repeatedly. The light blue region represents particles approaching while the laser was on. The light orange region represents particles repulsing each other. The red solid line indicates the slope of the separation curve at the moment of laser-off, corresponding to the release velocity $v_0(r) = \frac{dr}{dt}$ at various separation distances r . Note that the separation distance between particles was maintained at a finite value without attachment while the laser remained on. The same procedure was repeated many times for the same particle pair, and also repeated for several different particle pairs. The observed release velocity values are plotted as a function of separation distance r in Figure 5b. The release velocity v_0 was then converted to force using the Stokes drag force equation $F(r) = 6\pi R\eta_{eff}v_0(r)$ that corresponds to the repulsive force between the particles (Figure 5c). The effective viscosity could be approximated depending on the portion of a particle exposed to each fluid phase, given by $\eta_{eff} = [\eta_o(1 - \cos \theta_{ow}) + \eta_w(1 + \cos \theta_{ow})]/2$, [19-21] where $0.925 \text{ mPa} \cdot \text{s}$ was used for the oil viscosity value η_o , and $1.0 \text{ mPa} \cdot \text{s}$ was used for the water viscosity value η_w . The three-phase contact angle θ_{ow} at the oil–water interface was measured to be $\sim 130^\circ$ using the gel-trapping method. Each force data set was fitted with $F_{fit}(pN) = F_0 \left(\frac{2R}{r}\right)^4$, in which F_0 is the magnitude of the repulsive force.

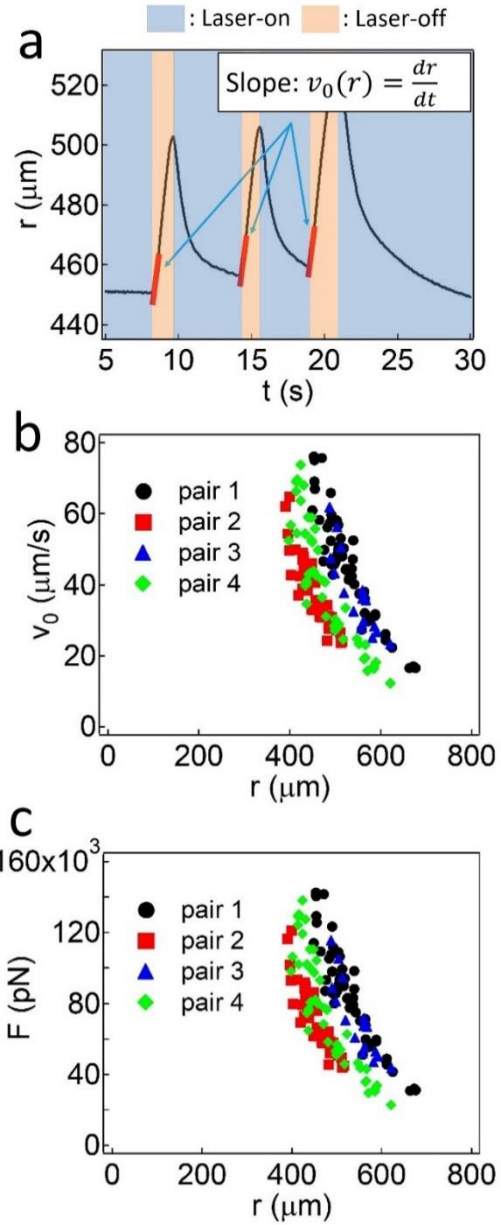


Figure 5. Indirect force measurements. (a) Interparticle distance r as a function of time, with a scenario in which the laser was turned on and then off three times. (b) Release velocities plotted as a function of r for all moments at which particles were released from optical force. Different symbols indicate four different particle pairs. (c) Electrostatic repulsive force calculated using the Stokes drag force equation.

Electrostatic repulsive force measured by direct/indirect measurements

The repulsive force was measured for many particle pairs of various diameters: $2R \approx 330$, 213, 117, and $84\text{ }\mu\text{m}$. For the small particles of diameter $2R \approx 3\text{ }\mu\text{m}$ (i.e., SPS and CPS), the time-sharing optical trap was employed to directly measure interaction force. The measured force was then normalized by F_0 and plotted as a function of $r/2R$ (Figures 6a and 6b). Regardless of the particle size, all of the experimental data points obtained from the two measurement methods conformed to the relationship of $F \sim r^{-4}$, which is a hallmark for electrostatic dipolar repulsion between colloidal particles at an oil–water interface [2, 10, 11]. Note that the capillary forces caused by either gravity or undulated meniscus were reported as attractive forces scaling respectively as r^{-1} or r^{-5} [12, 14, 50]. The scaling exponent of -4 obtained from the force measurements is strong evidence that capillary interactions of such large particles are negligible and that electrostatic repulsion dominates. The origin of the electrostatic repulsion can be attributed to the presence of PVA on the surface that was used as a stabilizer when the PS emulsion droplets were generated in the microfluidic channel [57]. Indeed, the PS/chloroform solution was emulsified in PVA-water by vortexing, under fluid conditions identical to those of the microfluidic protocol. After removing the solvent from the PS droplets, the measured ζ -potential was found to be in the range of $-30.9 \pm 0.87\text{ mV}$.

The interaction magnitude between particles of equal size depended on each particle pair. The error bars for mean magnitude of the interaction force $\langle F_0 \rangle$ in Figure 6c demonstrate the interaction heterogeneity that has been observed elsewhere previously [19, 21, 41, 42, 55, 60]. For particles fabricated by the microfluidic method, $\langle F_0 \rangle$ tended to increase with increasing particle size. This is likely because, for the case of particles made with the same protocol, the larger the particle, the more functional groups on the surface. Additionally, the lower effective surface-to-surface distance between larger particles at the same center-to-center separation distance tended to boost F_0 for larger particles relative to smaller particles.

On the other hand, measured $\langle F_0 \rangle$ values were similar for particles of diameter $2R \approx 330$ and those of diameter $213\text{ }\mu\text{m}$. We attribute this to differences in fabrication protocol. The total quantity of surface function groups (i.e., PVA) likely depends on the initial emulsion size and the polymer (PS) concentration in the emulsion droplets. It would be interesting to quantitatively investigate the relationship between surface charge, electrostatic repulsive force, and particle production protocol via the microfluidic method. However, such an investigation is outside the scope of the present study, and here we focus on clarifying the relative magnitudes of repulsive force and capillary force and their dependence on particle size.

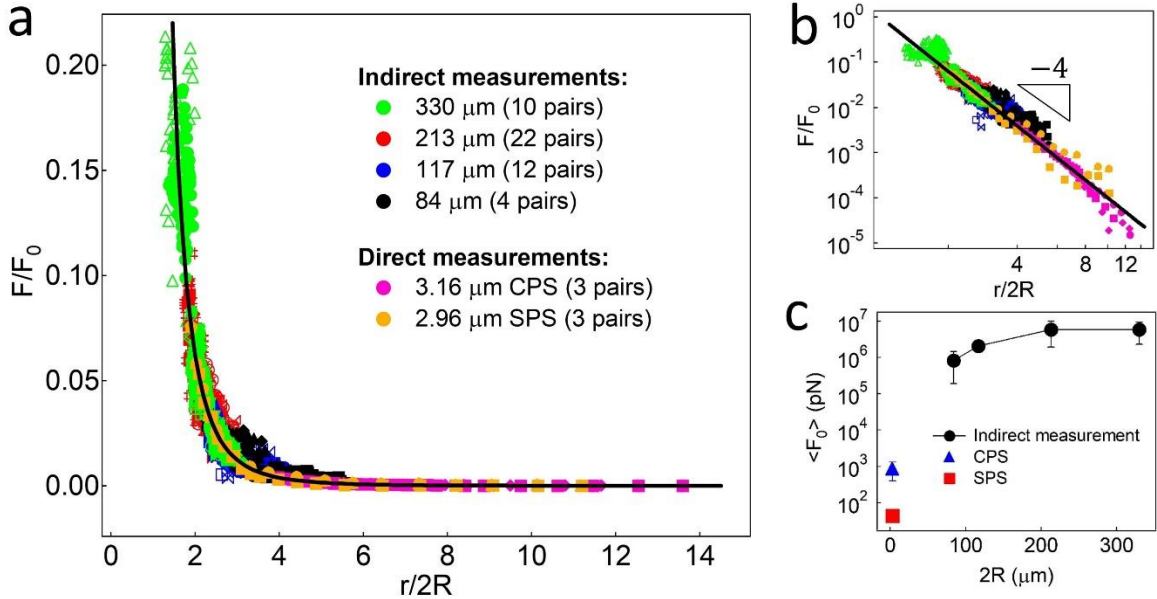


Figure 6. Electrostatic repulsive force measured by direct and indirect measurements. (a) Repulsive force normalized by F_0 as a function of $r/2R$. Different colors indicate different particle sizes. Different symbols of the same size denote different particle pairs. (b) The corresponding log-log plot. The solid line in panels a and b is the guide line for $F \sim r^{-4}$. (c) Mean magnitude of interaction force $\langle F_0 \rangle$ as a function of $2R$.

Conclusion. A brief paragraph that summarizes the major achievements of the research.

We quantitatively investigated the relative strengths of electrostatic repulsion and capillary attraction of PS particles at an oil–water interface. Regardless of particle size in the diameter range of $\sim 3 \mu\text{m} \leq 2R \leq \sim 330 \mu\text{m}$, the interaction force measured with optical laser apparatus was purely repulsive. The estimated capillary force caused by gravity-induced interface deformation was several orders of magnitude smaller than that of the measured repulsive force. This study empirically revealed that even for particles of diameters of several hundred micrometers, interparticle interaction can be dominated by electrostatic repulsive force, rather than by capillary force caused by interface deformation. In a subsequent study, we will focus on finely controlling particle size and surface charge in the microfluidic fabrication. Using these particles, we will quantitatively investigate the conditions under which electrostatic repulsive force does not dominate. We suggest using optical laser tweezers and laser microscopes to address the effect of the dipole component of meniscus undulation on capillary force and its dependence on particle size.

Acknowledgments.

Conflict of Interest Statement.

References.

1. Binks, B.P. and Horozov, T.S. (2006), Colloidal Particles at Liquid Interfaces: An Introduction., Eds., Colloidal Particles at Liquid Interfaces, Cambridge University Press, Cambridge, 1-74.
2. M. Oettel, S. Dietrich (2008), Colloidal interactions at fluid interfaces, Langmuir 24(4) 1425-1441.
3. R. McGorty, J. Fung, D. Kaz, V.N. Manoharan (2010), Colloidal self-assembly at an interface, Mater. Today 13(6) 34-42.
4. B.J. Park, D. Lee, Particles at fluid–fluid interfaces: From single-particle behavior to hierarchical assembly of materials, MRS Bull. 39(12) (2014) 1089-1098.
5. B.J. Park, D. Lee (2015), Dynamically Tuning Particle Interactions and Assemblies at Soft Interfaces: Reversible Order–Disorder Transitions in 2D Particle Monolayers, Small 11(35) 4560-4567.

6. B.J. Park, D. Lee, E.M. Furst (2015), CHAPTER 2 Interactions and Conformations of Particles at Fluid-Fluid Interfaces, Particle-Stabilized Emulsions and Colloids: Formation and Applications, The Royal Society of Chemistry, pp. 8-44.
7. N. Ballard, A.D. Law, S.A. Bon (2019), Colloidal particles at fluid interfaces: behaviour of isolated particles, *Soft matter* 15(6) 1186-1199.
8. B.P. Binks (2002), Particles as Surfactants-Similarities and Differences, *Curr. Opin. Colloid Interface Sci.* 7(1-2) 21-41.
9. R. Aveyard, J.H. Clint, D. Nees (2000), V.N. Paunov, Compression and Structure of Monolayers of Charged Latex Particles at Air/Water and Octane/Water Interfaces, *Langmuir* 16(4) 1969-1979.
10. A.J. Hurd(1985), The electrostatic interaction between interfacial colloidal particles, *J. Phys. A: Math. Gen.* 18(16) L1055-L1060.
11. P. Pieranski (1980), Two-Dimensional Interfacial Colloidal Crystals, *Phys. Rev. Lett.* 45(7) 569-572.
12. K.D. Danov, P.A. Kralchevsky, B.N. Naydenov (2005), G. Brenn, Interactions between particles with an undulated contact line at a fluid interface: Capillary multipoles of arbitrary order, *J. Colloid Interface Sci.* 287(1) 121-134.
13. J.C. Loudet, A.M. Alsayed, J. Zhang, A.G. Yodh (2005), Capillary Interactions Between Anisotropic Colloidal Particles, *Phys. Rev. Lett.* 94(1) 018301.
14. D. Stamou, C. Duschl, D. Johannsmann (2000), Long-range attraction between colloidal spheres at the air-water interface: The consequence of an irregular meniscus, *Phys. Rev. E* 62(4) 5263-5272.
15. P.A. Kralchevsky, N.D. Denkov, K.D. Danov (2001), Particles with an undulated contact line at a fluid interface: interaction between capillary quadrupoles and rheology of particulate monolayers, *Langmuir* 17(24) 7694-7705.
16. P.A. Kralchevsky, K. Nagayama (1994), Capillary forces between colloidal particles, *Langmuir* 10(1) 23-36.
17. B.J. Park, E.M. Furst (2011), Attractive interactions between colloids at the oil–water interface, *Soft Matter* 7(17) 7676-7682.
18. H. Rezvantalab, S. Shojaei-Zadeh (2013), Capillary interactions between spherical Janus particles at liquid–fluid interfaces, *Soft Matter* 9(13) 3640-3650.

19. B.J. Park, J. Vermant, E.M. Furst (2010), Heterogeneity of the electrostatic repulsion between colloids at the oil–water interface, *Soft Matter* 6(21) 5327-5333.
20. K. Masschaele, B.J. Park, E.M. Furst, J. Fransaer, J. Vermant (2010), Finite Ion-Size Effects Dominate the Interaction between Charged Colloidal Particles at an Oil-Water Interface, *Phys. Rev. Lett.* 105(4) 048303.
21. B.J. Park, J.P. Pantina, E.M. Furst, M. Oettel, S. Reynaert, J. Vermant (2008), Direct Measurements of the Effects of Salt and Surfactant on Interaction Forces between Colloidal Particles at Water–Oil Interfaces, *Langmuir* 24(5) 1686-1694.
22. C.L. Wirth, E.M. Furst, J. Vermant (2014), Weak electrolyte dependence in the repulsion of colloids at an oil–water interface, *Langmuir* 30(10) 2670-2675.
23. I. Buttinoni, Z.A. Zell, T.M. Squires, L. Isa (2015), Colloidal binary mixtures at fluid–fluid interfaces under steady shear: structural, dynamical and mechanical response, *Soft matter* 11(42) 8313-8321.
24. B. Madivala, J. Fransaer, J. Vermant (2009), Self-Assembly and Rheology of Ellipsoidal Particles at Interfaces, *Langmuir* 25 2718-2728.
25. K. Masschaele, J. Fransaer, J. Vermant (2009), Direct visualization of yielding in model two-dimensional colloidal gels subjected to shear flow, *J. Rheol.* 53(6) 1437-1460.
26. B.J. Park, T. Brugarolas, D. Lee (2011), Janus particles at an oil–water interface, *Soft Matter* 7(14) 6413-6417.
27. L. Botto, E.P. Lewandowski, M. Cavallaro, K.J. Stebe (2012), Capillary interactions between anisotropic particles, *Soft Matter* 8(39) 9957-9971.
28. E.P. Lewandowski, M. Cavallaro, L. Botto, J.C. Bernate, V. Garbin, K.J. Stebe (2010), Orientation and Self-Assembly of Cylindrical Particles by Anisotropic Capillary Interactions, *Langmuir* 26 15142-15154.
29. J. Vermant (2011), Fluid mechanics: When shape matters, *Nature* 476(7360) 286-287.
30. S. Reynaert, P. Moldenaers, J. Vermant (2006), Control over Colloidal Aggregation in Monolayers of Latex Particles at the Oil-Water Interface, *Langmuir* 22 4936-4945.

31. E.J. Stancik, M.J.O. Widenbrant, A.T. Laschitsch, J. Vermant, G.G. Fuller (2002), Structure and Dynamics of Particle Monolayers at a Liquid–Liquid Interface Subjected to Extensional Flow, *Langmuir* 18(11) 4372-4375.
32. K.J. Stebe, E. Lewandowski, M. Ghosh (2009), Oriented assembly of metamaterials, *Science* 325(5937) 159-160.
33. N. Laal-Dehghani, G.F. Christopher (2019), 2D Stokesian Simulation of Particle Aggregation at Quiescent Air/Oil-Water Interfaces, *J. Colloid Interface Sci.*.
34. S. Shahid, S.R. Gurram, M.G. Basavaraj (2018), Doubly pH Responsive Emulsions by Exploiting Aggregation of Oppositely Charged Nanoparticles and Polyelectrolytes, *Langmuir* 34(17) 5060-5071.
35. J. Faria, M.P. Ruiz, D.E. Resasco (2010), Phase-selective catalysis in emulsions stabilized by Janus silica-nanoparticles, *Adv. Synth. Catal.* 352(14-15) 2359-2364.
36. J. Frelichowska, M.-A. Bolzinger, J.-P. Valour, H. Mouaziz, J. Pelletier, Y. Chevalier (2009), Pickering w/o emulsions: Drug release and topical delivery, *Int. J. Pharm.* 368(1) 7-15.
37. B.P. Binks, R. Murakami (2006), Phase inversion of particle-stabilized materials from foams to dry water, *Nat. Mater.* 5(11) 865.
38. H. Son, H. Kim, G. Lee, J. Kim, W. Sung (2014), Enhanced oil recovery using nanoparticle-stabilized oil/water emulsions, *Korean J. Chem. Eng.* 31(2) 338-342.
39. M. Rayner, D. Marku, M. Eriksson, M. Sjöö, P. Dejmek, M. Wahlgren (2014), Biomass-based particles for the formulation of Pickering type emulsions in food and topical applications, *Colloids Surf. A* 458 48-62.
40. A.D. Dinsmore, M.F. Hsu, M.G. Nikolaides, M. Marquez, A.R. Bausch, D.A. Weitz (2002), Colloidosomes: Selectively Permeable Capsules Composed of Colloidal Particles, *Science* 298 1006-1009.
41. D.W. Kang, K.H. Choi, S.J. Lee, B.J. Park (2019), Mapping Anisotropic and Heterogeneous Colloidal Interactions via Optical Laser Tweezers, *Journal of Physical Chemistry Letters* 10(8) 1691-1697.
42. J.H. Lim, J.Y. Kim, D.W. Kang, K.H. Choi, S.J. Lee, S.H. Im, B.J. Park (2018), Heterogeneous Capillary Interactions of Interface-Trapped Ellipsoid Particles Using the Trap-Release Method, *Langmuir* 34(1) 384-394.

43. H. Lehle, E. Noruzifar, M. Oettel (2008), Ellipsoidal particles at fluid interfaces, *Eur. Phys. J. E*: 26(1-2) 151-160.
44. G.B. Davies, T. Krüger, P.V. Coveney, J. Harting, F. Bresme (2014), Assembling ellipsoidal particles at fluid interfaces using switchable dipolar capillary interactions, *Adv. Mater.* 26(39) 6715-6719.
45. A. Kumar, B.J. Park, F. Tu, D. Lee (2013), Amphiphilic Janus particles at fluid interfaces, *Soft Matter* 9(29) 6604-6617.
46. W. Chen, S. Tan, T.-K. Ng, W.T. Ford, P. Tong (2005), Long-ranged attraction between charged polystyrene spheres at aqueous interfaces, *Phys. Rev. Lett.* 95(21) 218301.
47. J.D. Feick, N. Chukwumah, A.E. Noel, D. Velegol (2004), Altering surface charge nonuniformity on individual colloidal particles, *Langmuir* 20(8) 3090-3095.
48. V. Carrasco-Fadanelli, R. Castillo (2019), Measurement of the force between uncharged colloidal particles trapped at a flat air/water interface, *Soft matter* 15(29) 5815-5818.
49. M.P. Boneva, K.D. Danov, N.C. Christov, P.A. Kralchevsky (2009), Attraction between particles at a liquid interface due to the interplay of gravity-and electric-field-induced interfacial deformations, *Langmuir* 25(16) 9129-9139.
50. D.Y.C. Chan, J.D. Henry, L.R. White (1981), The interaction of colloidal particles collected at fluid interfaces, *J. Colloid Interface Sci.* 79(2) 410-418.
51. N.D. Vassileva, D. van den Ende, F. Mugele, J. Mellema (2005), Capillary forces between spherical particles floating at a liquid– liquid interface, *Langmuir* 21(24) 11190-11200.
52. V. Paunov, P. Kralchevsky, N. Denkov, K. Nagayama (1993), Lateral capillary forces between floating submillimeter particles, *J. Colloid Interface Sci.* 157(1) 100-112.
53. C. Monteux, E. Jung, G. Fuller (2007), Mechanical properties and structure of particle coated interfaces: influence of particle size and bidisperse 2D suspensions, *Langmuir* 23(7) 3975-3980.

54. D.W. Kang, M. Lee, K.H. Kim, M. Xia, S.H. Im, B.J. Park (2017), Electrostatic interactions between particles through heterogeneous fluid phases, *Soft matter* 13(37) 6647-6658.
55. M. Lee, B.J. Park (2015), Heterogeneity of single-colloid self-potentials at an oil–water interface, *Soft matter* 11(45) 8812-8817.
56. M. Lee, M. Xia, B.J. Park (2016), Transition Behaviors of Configurations of Colloidal Particles at a Curved Oil-Water Interface, *Materials* 9(3) 138.
57. J.P. Pantina, E.M. Furst, Directed assembly and rupture mechanics of colloidal aggregates, *Langmuir* 20(10) (2004) 3940-3946.
58. A. Ashkin (1992), Forces of a single-beam gradient laser trap on a dielectric sphere in the ray optics regime, *Biophys. J.* 61(2) 569-582.
59. D.W. Kang, B.G. Park, K.H. Choi, J.H. Lim, S.J. Lee, B.J. Park (2018), Geometric Effects of Colloidal Particles on Stochastic Interface Adsorption, *Langmuir* 34(30) 8839-8847.
60. D.W. Kang, J.H. Lim, B.J. Park (2017), Heterogeneous interface adsorption of colloidal particles, *Soft matter* 13(36) 6234-6242.
61. C.A. Schneider, W.S. Rasband, K.W. Eliceiri (2012), NIH Image to ImageJ: 25 years of image analysis, *Nat. Meth.* 9 671-675.
62. H.E. Lee, K.H. Choi, M. Xia, D.W. Kang, B.J. Park (2019), Interactions between polystyrene particles with diameters of several tens to hundreds of micrometers at the oil-water interface, *Journal of Colloid and Interface Science*